
GAIA: A FOUNDATION MODEL FOR OPERATIONAL ATMOSPHERIC DYNAMICS

Ata Akbari Asanjan¹, Olivia Alexander¹, Tom Berg², Clara Zhang², Matt Yang², Jad Makki², Disha Shidham¹, Srijita Chakraborty¹, William Bender², Stephen Peng², Arun Ravindran², Olivier Raiman¹, David Potere², David Bell¹

¹Research Institute for Advanced Computer Science (RIACS) at Universities Research Space Association (USRA)

²BCG X AI Science Institute

{aakbariasanjan, oalexander, dshidham, schakraborty, dbell}@usra.edu

{berg.tom, zhang.clara, yang.matt, makki.jad, bender.william, peng.stephen, ravindran.arun, potere.david}@bcg.com

ABSTRACT

We present the GAIA (Geospatial Artificial Intelligence for Atmospheres) Foundation Model, a novel model that combines masked autoencoders (MAE) and self-Distillation with NO labels (DINO) for analyzing global atmospheric patterns in satellite imagery. By integrating these complementary self-supervised learning approaches, our model simultaneously captures both local features and global dependencies. We address two critical challenges in satellite data analysis: reconstructing missing regions and estimating precipitation patterns as our first downstream tasks. The model demonstrates superior temporal pattern capture compared to standard MAE approaches, while maintaining robust performance in downstream tasks. Our experimental results show strong gap-filling capabilities across varying mask ratios and accurate precipitation estimation with limited training data, achieving a false alarm ratio of 0.088 and structural similarity of 0.881. This work represents an advancement in self-supervised learning for atmospheric science, providing a foundation for improved weather monitoring and climate analysis. The trained model weights and accompanying code are publicly available as open-source on Hugging Face here: <https://huggingface.co/bcg-usra-nasa-gaia/GAIA-v1>.

Keywords Foundation Models · Satellite Imagery · Self-Supervised Learning · Gap Filling · Precipitation Estimation

1 Introduction

Satellite data analysis presents significant challenges in modern atmospheric science, particularly in processing and interpreting the vast volumes of data generated daily. Key challenges include understanding high-dimensional spatiotemporal patterns, managing missing or corrupted observations, and extracting meaningful features across multiple spatial and temporal scales [1, 2, 3]. Traditional approaches often struggle to capture the complex interplay between global atmospheric circulation patterns and local weather phenomena, making it difficult to fully leverage satellite data for weather and climate applications [1, 4].

The emergence of deep learning approaches has opened new possibilities for addressing these challenges by enabling automatic feature extraction and hierarchical representation learning [5, 6]. These methods can capture complex spatial and temporal patterns directly from raw observations, offering promising solutions for satellite data analysis [7, 8]. However, existing deep learning approaches often focus on either local or global patterns independently, missing the crucial interactions between different atmospheric scales.

GOES (Geostationary Operational Environmental Satellite) data represents a cornerstone of modern weather monitoring and forecasting systems, providing continuous observations of atmospheric conditions across large geographical regions [9, 4]. Through its extensive spatial coverage and high temporal resolution, GOES data supports a wide range of applications, from severe weather monitoring to precipitation estimation. For instance, GOES data contributes to tracking atmospheric rivers, estimating precipitation rates, and monitoring water vapor transport [10, 11]. The National

Weather Service utilizes GOES data for generating Atmospheric Motion Vectors, while various precipitation products, including NASA’s IMERG, incorporate GOES observations for improved accuracy [12, 13].

Current methods for satellite image processing often rely on traditional computer vision techniques or task-specific deep learning models [14, 15]. However, these approaches frequently struggle with the unique characteristics of satellite data, including irregular sampling patterns, varying spatial resolutions, and complex atmospheric physics. A fundamental challenge is the persistent issue of missing data, which can arise from sensor malfunctions, atmospheric interference, or data transmission errors [2, 3]. These gaps significantly impact the reliability of weather monitoring and forecasting systems, particularly during critical weather events. Additionally, accurate precipitation estimation from satellite imagery remains a crucial yet challenging task, requiring both high accuracy and robust feature extraction to support climate monitoring and weather forecasting.

Existing approaches to these challenges often fall short in several key aspects. First, traditional interpolation methods for handling missing data fail to capture complex atmospheric dynamics. Second, current precipitation estimation systems frequently rely on hand-crafted features or simplified physical models, limiting their ability to adapt to varying atmospheric conditions. Third, most approaches focus on either local or global patterns independently, missing the crucial interactions between different atmospheric scales.

Recent advances in foundation models, particularly Masked Autoencoders (MAE) [16] and DINO (self-Distillation with NO labels) [17], have demonstrated remarkable success in learning rich, transferable representations from large-scale image data. MAEs excel at learning structural patterns by reconstructing images from partially masked inputs, while DINO enables the learning of semantic features through self-supervised training [18]. While these architectures have shown promise individually, their combined potential for satellite data analysis remains unexplored.

In this paper, we propose the GAIA Foundation Model, a novel hybrid architecture that combines the strengths of MAE and DINO approaches. Our model leverages the self-supervised learning capabilities of MAE for robust feature extraction from incomplete data, while incorporating DINO’s semantic learning framework to enhance the model’s understanding of atmospheric patterns. This hybrid approach enables more effective handling of missing data while maintaining high performance in precipitation estimation.

Our key innovations include: (1) a novel attention mechanism designed specifically for satellite imagery that captures both local and global atmospheric patterns, (2) an adaptive masking strategy that improves the model’s resilience to missing data, and (3) a unified learning framework that enables effective transfer to downstream tasks. The main contributions of our work are threefold: First, we introduce a novel foundation model architecture specifically designed for satellite data analysis, incorporating both global and local attention mechanisms. Second, we achieve robust precipitation estimation through our pre-trained architecture, enabling accurate predictions even with limited fine-tuning data.

The remainder of this paper is organized as follows: Section 2 reviews related work and background. Section 3 details our model architecture and training methodology. Section 4 provides comprehensive results and analysis of our model’s performance across various tasks. Finally, Section 5 concludes with a summary of our contributions and directions for future research.

2 Related Work

2.1 Foundation Models in Computer Vision

Autoencoders are neural network architectures that learn salient features of a dataset by projecting the input data into a lower dimensional space (deriving embeddings) using an encoder, followed by reconstructing the embedding into the original space using a decoder [19]. As the data is compressed into the embedding which is then reconstructed, the most characteristic properties of the data is learned during training. These models are naturally suited for tasks like cloud segmentation, atmospheric feature detection, and data denoising, where the goal is to distill essential structures from high-dimensional satellite inputs. Early uses of convolutional autoencoders demonstrated promise in extracting low-dimensional representations of satellite images for reconstruction and anomaly detection [14, 15]. The encoder maps spatial observations into a latent space, while the decoder reconstructs key atmospheric patterns, effectively learning a hierarchical representation that preserves geophysical meaning.

Masked autoencoders (MAE) applies self-supervised pre-training, where it masks random patches in the input and then learns to reconstruct it using an asymmetric encoder-decoder architecture based on the attention mechanism [16]. Specifically, the MAE uses the Vision Transformer (ViT) backbone [18]. The ViT encoder operates on the unmasked or visible patches only. A very high masking ratio (75%) is used to hide a large portion of the image and the unmasked patches are passed through a learnable linear projection layer and positional embeddings are added. The patch and

positional embeddings of the visible tokens are passed through transformer blocks where the relation between the patches is learned through self-attention and compressed to encoder embeddings. The decoder is lightweight and takes in both masked and unmasked tokens, along with their positional embeddings, and processes them through transformer blocks. It is then trained to reconstruct the pixels in each masked patch by minimizing the mean squared error (MSE) loss. Once trained, the pre-trained model and its encoder embeddings are generalizable to diverse downstream tasks [16].

In parallel, DINO (self-Distillation with NO labels) represents another significant advancement in self-supervised visual learning [17]. DINO employs a teacher-student architecture where both networks share the same Vision Transformer backbone but maintain different sets of parameters. The student network processes augmented views of the input image, while the teacher network, whose parameters are an exponential moving average of the student's, provides target representations [17]. The framework uses a local-to-global correspondence learning strategy, where local features from the student network are matched with global features from the teacher network. This approach enables the model to learn semantic correspondences without requiring explicit labels [20]. DINO's success lies in its ability to learn meaningful visual features that exhibit properties such as semantic correspondence and scene understanding, making it particularly valuable for tasks requiring semantic interpretation of visual data [17].

Recent advances in foundation models have demonstrated the effectiveness of hybrid architectures that combine multiple learning paradigms [21]. These hybrid approaches, particularly those integrating masked autoencoding with self-supervised learning techniques, have shown remarkable success in learning robust and transferable representations [22]. The combination of local and global attention mechanisms, coupled with hierarchical feature learning, enables these models to capture both fine-grained details and broader contextual information [23]. This architectural synergy has proven particularly advantageous in handling complex visual data with varying scales and temporal dependencies, making them well-suited for atmospheric science applications [24].

2.2 Satellite Image Analysis and Gap Filling

Traditional approaches to satellite image processing have relied on physical models and statistical methods [2]. However, the complexity of atmospheric phenomena and the high dimensionality of satellite data have motivated the development of deep learning-based solutions [1]. Recent advances in computer vision have led to significant improvements in satellite data processing, particularly in handling multi-spectral and multi-temporal data [6].

Gap filling in satellite imagery presents unique challenges due to the complex spatiotemporal nature of atmospheric data [25]. Traditional interpolation methods, while computationally efficient, often fail to capture the intricate patterns and physical constraints inherent in atmospheric data [26]. Deep learning approaches have shown promising results, with various architectures proposed for handling missing data in satellite observations [27]. These include convolutional neural networks for spatial interpolation [28], attention-based models for capturing long-range dependencies [25], and physics-informed neural networks that incorporate domain knowledge [29]. These approaches leverage the ability of neural networks to learn complex spatial and temporal correlations, enabling more accurate reconstruction of missing data.

2.3 Precipitation Estimation from Satellite Data

Precipitation estimation from satellite data has evolved significantly with the advancement of deep learning techniques [30]. Traditional methods relied heavily on infrared brightness temperature thresholds and empirical relationships [31]. Modern approaches leverage multiple data sources and advanced machine learning techniques to improve accuracy [12]. The PERSIANN family of algorithms demonstrates the evolution from simple neural networks to sophisticated deep learning architectures [32, 33]. Recent work has focused on incorporating multiple satellite sources, including both infrared and microwave observations, to enhance estimation accuracy [34]. Challenges in this domain include handling the spatial and temporal heterogeneity of precipitation patterns, dealing with different sensor characteristics, and maintaining physical consistency in the estimates [35].

2.4 Self-Supervised Learning in Remote Sensing

Self-supervised learning has emerged as a powerful paradigm in remote sensing applications, offering novel solutions to the challenges of large-scale satellite data analysis [36]. Recent studies have demonstrated its effectiveness in learning meaningful representations from unlabeled satellite imagery through various pretext tasks, including temporal prediction, spatial reconstruction, and multi-modal alignment [37]. These approaches have been particularly successful in extracting spatiotemporal patterns from geostationary satellite data, enabling improved weather pattern recognition and atmospheric state prediction [11].

However, satellite imagery presents unique challenges that distinguish it from traditional computer vision tasks [3]. These include the presence of complex atmospheric physics, varying spatial resolutions across different spectral bands, and the inherent multi-scale nature of atmospheric phenomena [2]. Additionally, satellite data often exhibits systematic gaps due to sensor limitations, cloud cover, and orbital characteristics, necessitating robust learning approaches that can handle missing or corrupted observations [25].

Current self-supervised learning approaches in remote sensing face several limitations. First, most existing methods focus on single-task learning, lacking the ability to learn generalizable representations that can benefit multiple downstream tasks [21]. Second, the computational complexity of processing high-dimensional satellite data at global scales remains a significant challenge, often requiring trade-offs between spatial resolution and temporal coverage [8]. Third, the integration of domain-specific physical constraints and prior knowledge into self-supervised learning frameworks remains an open challenge, particularly for applications requiring physical consistency in predictions [1].

3 Methodology

3.1 Data

The Geostationary Operational Environmental Satellite (GOES) dataset provides high-resolution, high-temporal-frequency satellite imagery critical for weather forecasting, climate monitoring, and atmospheric research. Operated by NOAA, the GOES series delivers data across multiple spectral bands, including visible, infrared, and water vapor channels. In this work, we use brightness temperature data from the cloud top temperature product, primarily derived from GOES Channel 13 (10.3 μm), part of the longwave infrared band. The native dataset contains imagery at 4 km spatial resolution with snapshots of the globe every 30 minutes. Prior to training, we downscale the images to 480×1440 pixels (approximately 28 km per pixel or 0.25 degrees) to reduce computational complexity while retaining sufficient spatial information. Even after downscaling, the imagery remains high-dimensional and structurally rich—highlighting the need for a powerful foundational model to fully interpret it.

Our preprocessing pipeline involves a two-step approach to handle missing data. First, we apply a bidirectional fill using linear interpolation within a 5-pixel radius in both latitude and longitude directions to address small voids in the data. This initial step helps maintain spatial continuity for minor gaps. Larger missing regions that cannot be filled through this local interpolation are preserved and later incorporated into our masking strategy during training.

Despite its richness, the GOES dataset frequently includes missing regions caused by sensor dropouts, calibration issues, or limited scene coverage. On average, about 7.5% of pixels are missing in GOES imagery.¹ An important objective of GAIA is to fill in the missing gaps in GOES data, using its understanding of global weather dynamics.

3.2 Model Architecture

Our hybrid architecture (illustrated in Figure 2) integrates MAE and DINO frameworks through a shared encoder, enabling simultaneous learning of local and global features. The architecture consists of three main components:

1. A shared ViT-based encoder that processes patches from both MAE and DINO branches
2. A lightweight decoder for reconstruction in the MAE branch
3. A momentum-updated teacher network for self-distillation in the DINO branch

The encoder follows the Vision Transformer architecture with an embedding dimension of 912 (matching our $30 \times 30 \times 1$ patch size), 24 layers, and 16 attention heads. The decoder is more lightweight, with an embedding dimension of 512, 8 layers, and 16 attention heads. This asymmetric design allows for efficient computation while maintaining high reconstruction quality.

During pre-training, we employ a 75% masking ratio, where both the MAE and DINO branches see different randomly masked versions of the same input. The MAE branch’s mask is shared with the student network (shared encoder) to ensure consistency in the learning process. The teacher network in the DINO branch is updated using a momentum coefficient of 0.996, promoting stable learning of global features.

¹For 1000 randomly sampled images between 2005 and 2015, the average missing data amount of 7.5% of pixels. Note that this is calculated after our data-preprocessing steps, which includes filling missing data pixels with the nearest non-missing pixel if there is a non-missing pixel within 5 pixels vertically or horizontally. So, the missing data amount in the raw data is greater than this.

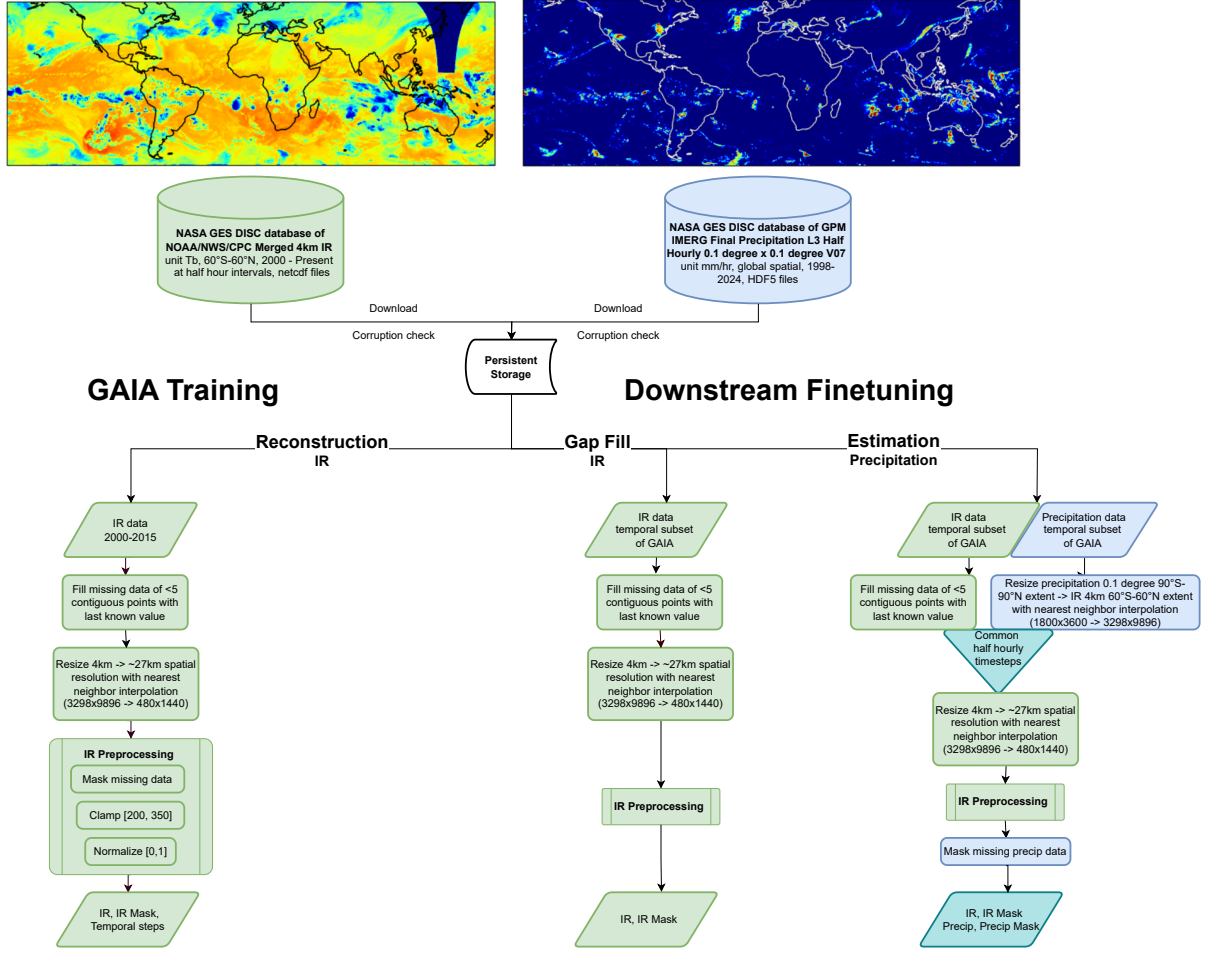


Figure 1: Data Preprocessing Pipeline: The raw GOES data undergoes spatial downscaling followed by a two-step missing data handling process - local interpolation for small gaps and preservation of larger gaps for the masking strategy.

3.3 Training Strategy

Our training strategy involves two phases: pre-training of the base model followed by task-specific fine-tuning. For pre-training, we utilize 15 years of GOES data (2001-2015) at 0.25-degree resolution. The model is trained using Bfloat16 precision to optimize memory usage and computational efficiency.

The MAE reconstruction loss is defined as:

$$\mathcal{L}_{\text{MAE}} = \frac{1}{|M|} \sum_{i \in M} \|x_i - \hat{x}_i\|_2^2 \quad (1)$$

where M is the set of masked patches, x_i is the original patch, and \hat{x}_i is the reconstructed patch.

The pre-training objective combines the MAE reconstruction loss (Equation 1) with the DINO loss. For the DINO component, we use a student temperature of 0.1 and a teacher temperature of 0.04, with a center momentum of 0.9. The learning rate follows a cosine annealing schedule starting from $1e-3$.

For downstream tasks, we fine-tune the model with task-specific modifications:

- **Gap Filling:** We reduce the masking ratio to 10% during fine-tuning while allowing the encoder to adapt. The loss function combines MSE for both visible and masked patches, excluding naturally missing regions from the calculation.

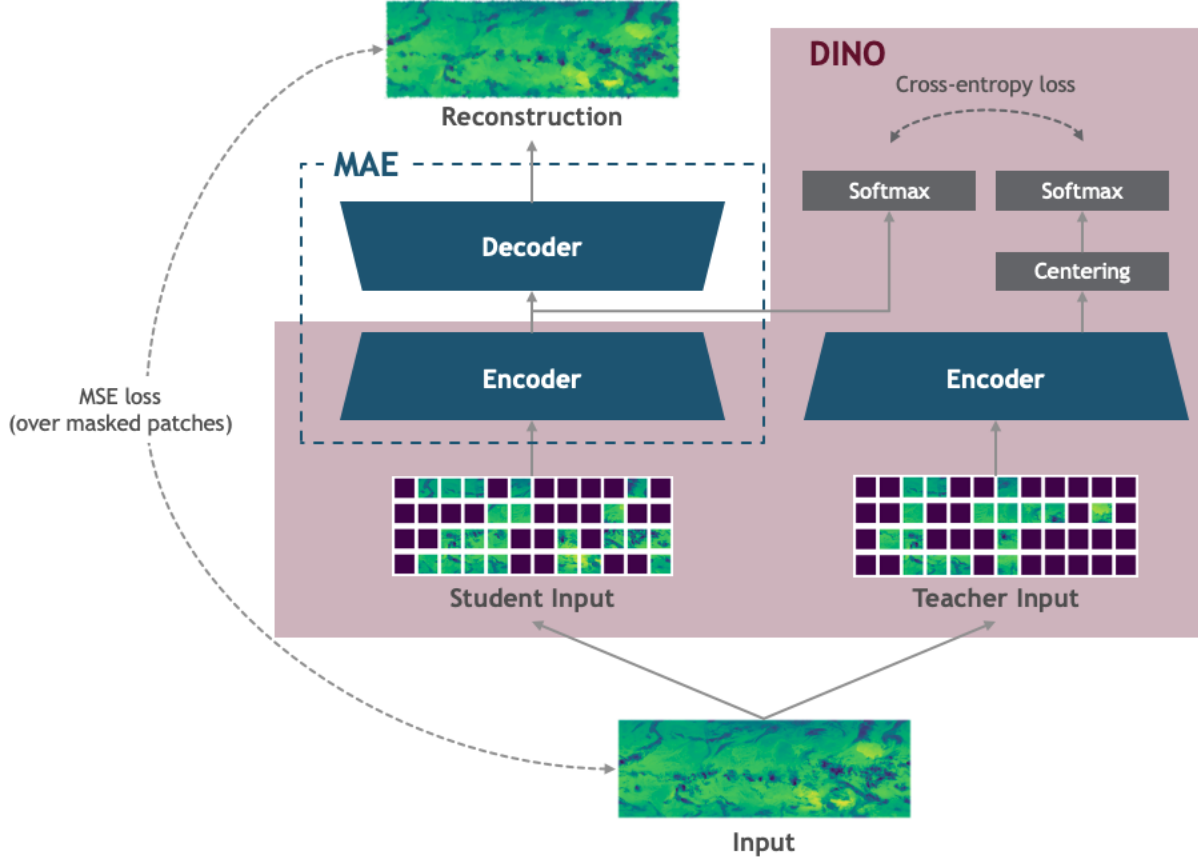


Figure 2: Architecture overview of the MAE-DINO (Masked Autoencoder with self-distillation) framework. The model combines two powerful self-supervised learning approaches: (a) MAE (Masked Autoencoder), which randomly masks patches of the input image and learns to reconstruct the missing regions, and (b) DINO (Distillation with No Labels), which uses a teacher-student architecture for knowledge distillation. The encoder processes visible patches (75% of image) through a series of transformer blocks, while the lightweight decoder reconstructs the full image from visible tokens. This architecture enables efficient self-supervised pretraining on large-scale datasets without requiring manual labels, leading to robust visual representations that can be fine-tuned for downstream tasks.

- **Precipitation Estimation:** We maintain the 10% masking ratio and add a ReLU activation in the output layer to ensure non-negative precipitation estimates. The model is fine-tuned using two months of data, with MSE loss calculated similarly to the gap-filling task.

3.4 Hardware and Computational Requirements

The GAIA model was trained and evaluated on the National Research Platform (NRP), a distributed Kubernetes cluster accessible across U.S. universities.

The computational infrastructure utilized NVIDIA A10 GPUs located at UNL (University Nebraska Lincoln), with the training process configured for distributed training across multiple nodes. Key training parameters were managed through a Kubernetes job specification, allowing for flexible allocation of resources.

GAIA was trained on 9 nodes, each with 8 NVIDIA A10 GPUs (72 in total), using DeepSpeed Stage 2 for distributed training in bf16 mixed precision. The global batch size was 144 (with a micro-batch of 1 per GPU and 2 gradient accumulation steps). We used the AdamW optimizer with an initial learning rate of $5e-4$ and applied a cosine annealing scheduler. The GAIA base model was trained for 34,585 steps over approximately 5.8 days.

3.5 Downstream Tasks

3.5.1 Gap Filling

The gap-filling model builds upon our pre-trained architecture with several modifications. We maintain the same encoder-decoder structure but reduce the masking ratio to 10% during fine-tuning. This lower ratio helps the model focus on realistic gap patterns while still providing sufficient learning signal through artificial masking. The loss function combines MSE terms for both visible and masked patches, enabling the model to reconstruct the entire image as opposed to only masked patches:

$$\mathcal{L}_{\text{gap}} = \frac{1}{|V|} \sum_{i \in V} \|x_i - \hat{x}_i\|_2^2 + \frac{1}{|M|} \sum_{i \in M} \|x_i - \hat{x}_i\|_2^2 \quad (2)$$

where V and M represent the sets of visible and artificially masked patches respectively, excluding naturally missing regions from the calculation.

3.5.2 Precipitation Estimation

For precipitation estimation, we extend the gap-filling architecture by adding a ReLU activation in the output layer to ensure physically meaningful (non-negative) precipitation estimates. The model is fine-tuned using two months of data from 2005 and evaluated on 2020 data to assess both its reconstruction and estimation capabilities.

The precipitation estimation task presents unique challenges due to the non-linear relationship between infrared brightness temperatures and precipitation rates. Our architecture addresses this by:

- Maintaining the encoder’s pre-trained understanding of atmospheric patterns
- Using the 10% masking ratio to ensure robust performance with missing data
- Applying ReLU activation to enforce physical constraints
- Computing MSE loss over both visible and masked regions

The model’s performance is evaluated using multiple metrics including False Alarm Ratio (FAR), Pixel Accuracy, RMSE, and SSIM, providing a comprehensive assessment of both reconstruction quality and precipitation estimation accuracy.

4 Experiments and Results

4.1 Temporal Pattern Analysis

We analyze how well each model captures temporal dependencies by examining embedding differences over time (Figure 3) for a MAE-only model compared to a MAE-DINO model. Our experiments utilize one year of GOES satellite data for pre-training, with model checkpoints selected at convergence based on validation performance.

MAE-DINO demonstrates consistent alignment with input data changes across the temporal dimension, maintaining stable embedding differences that correlate well with actual temporal changes in satellite imagery. In contrast, MAE shows a characteristic peak at the 12-hour mark followed by a decline, suggesting a focus on local temporal patterns driven by diurnal cycles rather than broader atmospheric dynamics.

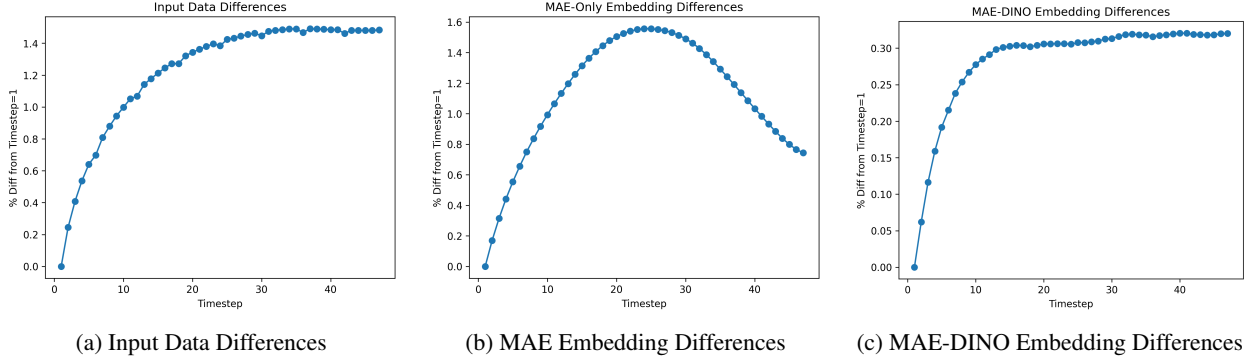


Figure 3: Temporal pattern analysis comparing how input data differences and model embeddings evolve over time. Input data (left) shows natural temporal evolution, MAE embeddings (middle) exhibit strong diurnal cycle influence with a peak at 12 hours, while MAE-DINO embeddings (right) maintain consistent temporal pattern capture aligned with input changes. Note that each day has 48 timesteps at 30-minute increments. Timestep 24 represents 12 hours into a day.

4.2 Downstream Task Evaluation

4.2.1 Gap Filling Evaluation

We evaluate GAIA’s ability to reconstruct missing regions in global satellite imagery, a critical task for handling sensor malfunctions or data transmission issues. The model was trained with a 10% mask ratio, striking a balance between learning robust representations and maintaining computational efficiency. The model is trained to both reconstruct the visible patches in the input image and fill in missing data gaps.

Figure 4 demonstrates the model’s gap filling and reconstruction capabilities across three challenging scenarios. Each row presents a pair of images: the ground truth (left) with missing data (shown in dark blue) and the model’s reconstruction (right).

The results showcase several key strengths of our approach:

- **Large Gap Reconstruction:** The model successfully reconstructs substantial missing regions while preserving the temperature gradients and atmospheric patterns consistent with surrounding areas.
- **Pattern Continuity:** The reconstructions maintain smooth transitions between filled regions and original data, avoiding artificial boundaries or discontinuities.
- **Detail Preservation:** Fine-scale features such as cloud formations and temperature variations are accurately reproduced, suggesting the model has learned meaningful representations of atmospheric physics rather than simple interpolation.
- **Visible Patch Reconstruction:** The fact that the model’s reconstruction closely replicates the fine-grained details in the input image suggests that the encoder is generating rich latent representations that can be reconstructed by the decoder.

We quantitatively evaluate GAIA’s gap filling ability by synthetically masking 100 samples taken from the full year of 2020 and computing the Root Mean Square Error (RMSE) and Structural Similarity Index (SSIM) between the gap-filled images from the model and the ground truth before synthetic masking. To simulate real-world data gaps, we selected four examples in our training data with significant missing data and used the missing pixels in those examples as our synthetic masks. Figure 5 plots the four synthetic masks we used.

Our results are shown in Table 1. The model’s high SSIM and low RMSE indicates strong gapfill performance across all four synthetic masks.

Despite being trained with only a 10% mask ratio, we also evaluate our model by running inference with varying artificial mask ratios to test its robustness. Figure 6 shows how reconstruction quality varies with mask ratio. The figure shows that as the mask ratio increases (less context available to the encoder), MSE for the artificially masked patches increases, indicating degraded reconstruction quality. This behavior is intuitive - with more patches hidden, the model has less contextual information to guide its predictions. However, even at higher mask ratios, the model maintains reasonable reconstruction quality, demonstrating its robustness in handling significant data gaps.

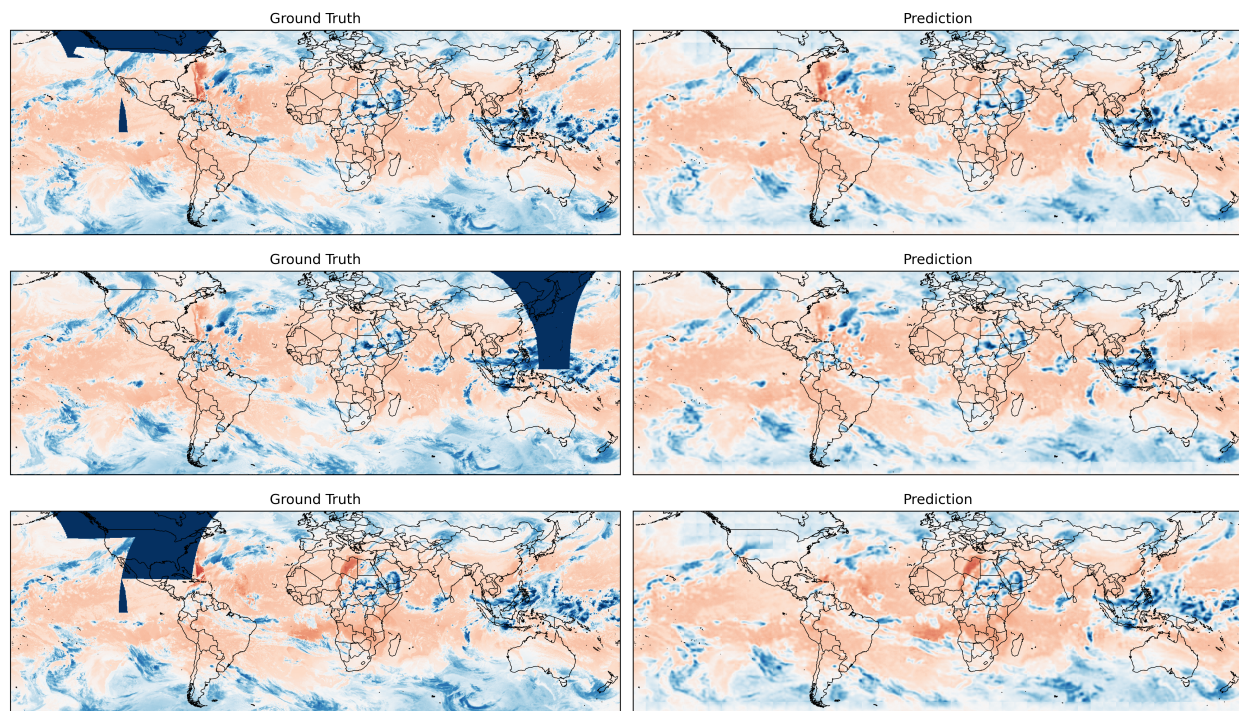


Figure 4: Comparison of ground truth (left) and reconstruction (right) across three different timestamps in 2015. The model successfully reconstructs missing regions (dark blue in ground truth) while preserving both spatial patterns and temperature intensity distributions.

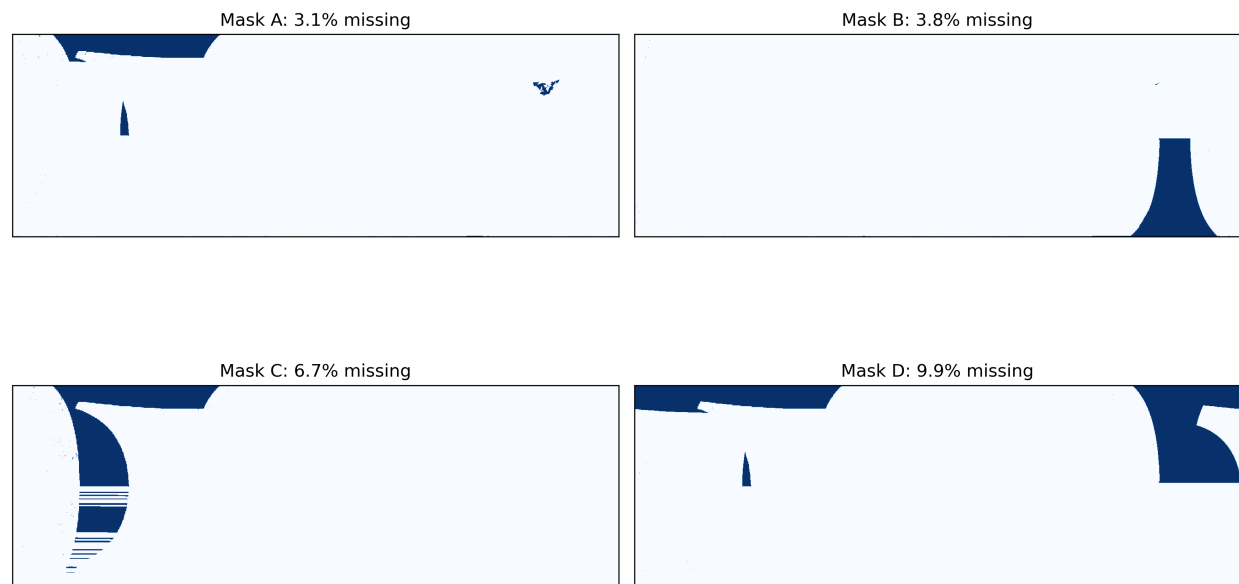


Figure 5: Visualization of the four synthetic masks used to test GAIA's gap filling capabilities. Blue indicates missing pixels, while white indicates available data.

These results demonstrate GAIA's effectiveness in handling real-world scenarios where satellite data may be partially missing or corrupted, providing a reliable solution for maintaining continuous global climate monitoring.

Mask	% missing	SSIM	RMSE
A	3.1%	0.814	0.051
B	3.8%	0.692	0.100
C	6.7%	0.776	0.070
D	9.9%	0.670	0.089

Table 1: Gap-filling performance metrics for 2020. We compute SSIM and RMSE over the synthetically masked portions of the data.

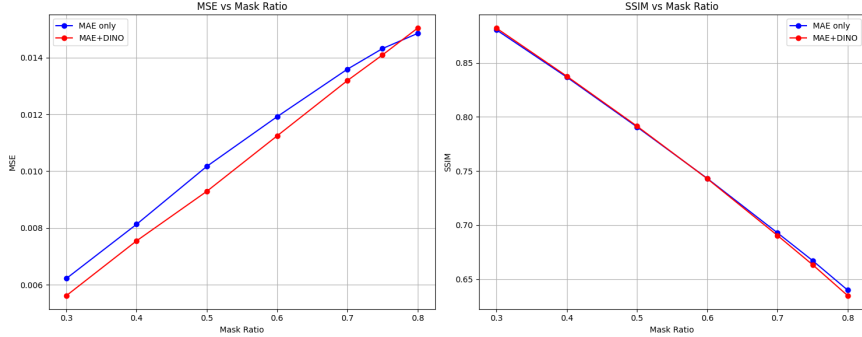


Figure 6: Quantitative evaluation of gap filling quality across different mask ratios. Mean Squared Error (MSE) (Left subplot) increases, and Structural Similarity Index Measure (SSIM) (Right subplot) decreases with higher mask ratios for both MAE and MAE-DINO.

4.2.2 Precipitation Estimation Evaluation

We trained our GAIA precipitation estimation model on two months of data from 2005 and evaluated its performance across the full year of 2020. To quantify the model’s accuracy and reliability, we computed four key evaluation metrics: False Alarm Ratio (FAR), Pixel Accuracy, RMSE, and SSIM, as shown in Table 2.

Both metrics of FAR and Pixel Accuracy treat our precipitation task as binary classification of precipitation/no-precipitation. FAR should be low, indicating fewer false positives—i.e., the model rarely predicts rain when there is none. A FAR of 0.088 suggests a strong ability to avoid false alarms. Pixel Accuracy measures overall classification correctness across all pixels and should be high. A score of 0.835 indicates that the model correctly labels precipitation/no-precipitation for a large majority of pixels. RMSE quantifies the average magnitude of prediction errors in millimeters; lower values indicate better performance. Our RMSE of 0.768 mm reflects a relatively small error margin in predicted precipitation intensity. SSIM compares the predicted and ground truth images for structural similarity, where values close to 1 are ideal. Our SSIM of 0.881 shows that the spatial structure and intensity patterns of precipitation are well captured.

Metric	Value
False Alarm Ratio (FAR)	0.088
Pixel Accuracy	0.835
RMSE (mm)	0.768
SSIM	0.881

Table 2: Precipitation Estimation Performance Metrics for 2020. The model shows strong performance across all metrics, particularly in false alarm ratio and structural similarity, indicating reliable precipitation detection and pattern reproduction.

Together, these evaluation metric results suggest the model generalizes well from a limited training window (2 months in 2005) to long-term evaluation (all of 2020), maintaining good accuracy, structural realism, and low false positives in its precipitation predictions.

Figure 7 presents a visual comparison between the ground truth precipitation maps and the model’s corresponding predictions at three representative timestamps from 2020. Each row displays one timestamp, with the left column showing the true observed precipitation and the right column showing the model’s estimation. The model effectively captures the spatial distribution and intensity patterns of precipitation across a variety of atmospheric scenarios. In particular, it reconstructs core precipitation regions with good structural similarity, aligning with the high SSIM and low RMSE metrics reported earlier. Some finer spatial features may be smoothed in the predictions, but the broader storm patterns and coverage areas are well-preserved.

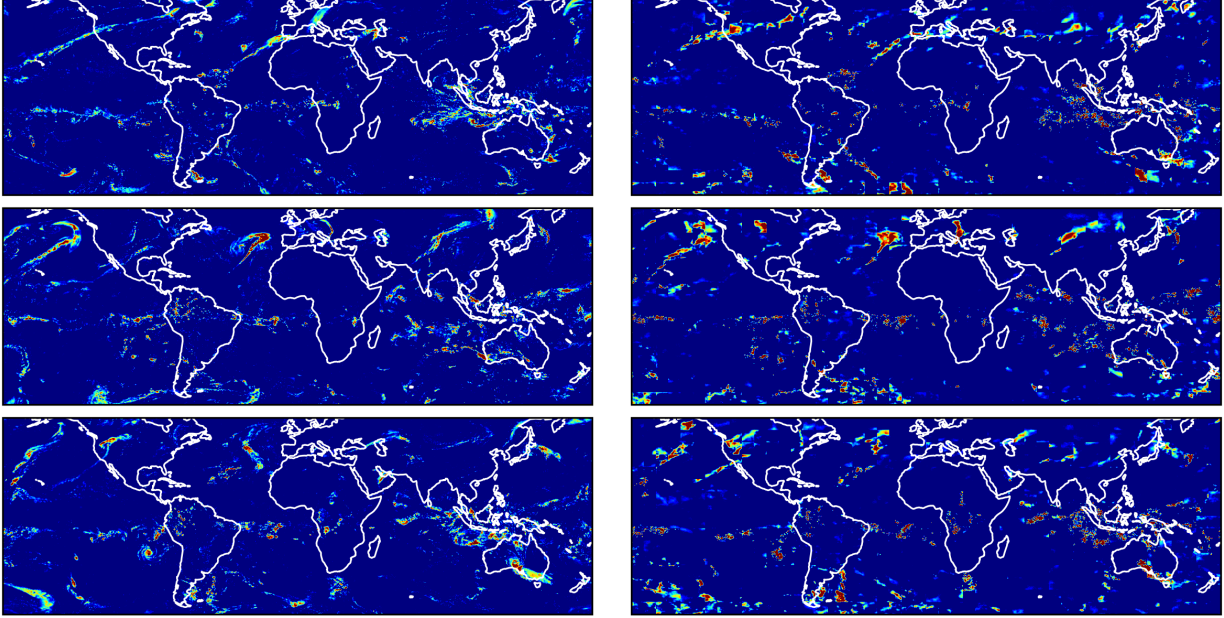


Figure 7: Comparison of ground truth (left) and model-estimated precipitation (right) for three timestamps in 2020. Each row corresponds to a specific time (Top to Bottom: October 11, 2020 at 05:00; July 2, 2020 at 02:30; October 8, 2020 at 02:30). Column 1 shows the ground truth precipitation, and Column 2 shows the corresponding model estimates.

These results demonstrate that the enhanced global context understanding provided by the MAE-DINO architecture translates effectively to downstream tasks, particularly in capturing complex atmospheric phenomena like precipitation patterns. The model’s ability to generalize from limited training data (2 months) to a full year of unseen data while maintaining high performance metrics suggests robust feature learning during the pre-training phase.

5 Conclusion

In this work, we introduced GAIA, a novel self-supervised learning framework that successfully combines MAE and DINO architectures to learn robust representations from satellite imagery. Our experimental results demonstrate several key achievements:

First, the integration of MAE’s reconstruction capabilities with DINO’s global attention mechanism yields representations that capture both local details and global atmospheric patterns. The enhanced attention distribution enables better understanding of long-range dependencies, as evidenced by the model’s superior performance in capturing temporal patterns beyond diurnal cycles. This is particularly significant for atmospheric science applications where global phenomena often influence local weather patterns.

Second, GAIA demonstrates remarkable effectiveness in practical applications with minimal fine-tuning requirements. In gap filling tasks, the model successfully reconstructs large missing regions while preserving complex atmospheric patterns and maintaining physical consistency. For precipitation estimation, even with limited training data (2 months), the model achieves strong performance across multiple metrics, including a low false alarm ratio of 0.088 and high structural similarity of 0.881.

The framework’s versatility extends beyond these demonstrated applications. GAIA’s learned representations are well-suited for various downstream tasks critical to atmospheric science, including:

- Tropical cyclone detection and segmentation
- Atmospheric river identification and tracking
- Weather pattern forecasting
- Other extreme weather event monitoring

While our results are promising, we acknowledge several areas for future improvement and development. The integration of weather simulation data as auxiliary training information could enhance the model’s understanding of atmospheric dynamics. This could be particularly valuable for capturing rare events or extreme conditions not well-represented in observational data. Additionally, while our current results demonstrate strong performance with limited fine-tuning data, exploring the model’s capabilities with higher spatial resolution inputs could further improve detail capture in downstream tasks.

The broader impact of this work extends beyond technical achievements. GAIA’s ability to handle missing data and identify weather patterns has significant implications for:

- Climate change monitoring: Providing continuous, gap-free satellite observations for tracking long-term climate trends
- Disaster preparedness: Early detection and tracking of extreme weather events
- Agricultural planning: Better precipitation forecasting for crop management
- Resource allocation: Improved weather prediction for renewable energy planning and water resource management

Looking ahead, we envision several promising directions for future research. The framework can be extended to incorporate multi-modal data sources, including simulation outputs for better physical consistency. The architecture’s flexibility allows for adaptation to additional downstream tasks, particularly in extreme weather event detection and prediction. Furthermore, the demonstrated efficiency in transfer learning suggests potential applications in regions with limited observational data.

In conclusion, GAIA represents a significant step forward in applying self-supervised learning to atmospheric science. By combining the strengths of MAE and DINO architectures, we have created a versatile framework that not only advances the technical capabilities of satellite image analysis but also provides practical tools for addressing critical environmental challenges.

Acknowledgments

This work used resources available through the USRA Research Institute for Advanced Computer Science (RIACS) and the National Research Platform (NRP) at the University of California, San Diego. NRP has been developed, and is supported in part, by funding from National Science Foundation, from awards 1730158, 1540112, 1541349, 1826967, 2112167, 2100237, and 2120019, as well as additional funding from community partners. The author(s) would like to thank Will Bender, Stephen Peng, Alexander Lobo, Evan Muscatel, An Nguyen, Sam Solovy, Claudia Jimenez Arellano, Besart Mujeci, and Dima Mishin for their invaluable help and insightful discussions throughout the development of this work.

References

- [1] Markus Reichstein and et al. Deep learning and process understanding for data-driven earth system science. *Nature*, 566(7743):195–204, 2019.
- [2] Bruce A Wielicki, DF Young, MG Mlynyczak, KJ Thome, S Leroy, J Corliss, JG Anderson, CO Ao, R Bantges, F Best, et al. Achieving climate change absolute accuracy in orbit. *Bulletin of the American Meteorological Society*, 94(10):1519–1539, 2013.
- [3] Oleg Dubovik, Gregory L Schuster, Feng Xu, Yongxiang Hu, Hartmut Bösch, Jochen Landgraf, and Zhengqiang Li. Grand challenges in satellite remote sensing, 2021.
- [4] Wenze Yang, Viju O John, Xuepeng Zhao, Hui Lu, and Kenneth R Knapp. Satellite climate data records: Development, applications, and societal benefits. *Remote Sensing*, 8(4):331, 2016.

- [5] Michel Besserve and et al. Variational latent state forecasting for spatiotemporal processes. In *ICLR*, 2021.
- [6] Sourav Ghosh and et al. Deep learning architectures for satellite image reconstruction. *IEEE Transactions on Geoscience and Remote Sensing*, 2022.
- [7] Stephan Rasp, Peter D Dueben, Sebastian Scher, Jonathan A Weyn, Soukayna Mouatadid, and Nils Thuerey. Weatherbench: A benchmark dataset for data-driven weather forecasting. *Journal of Advances in Modeling Earth Systems*, 12(11):e2020MS002203, 2020.
- [8] Thorsten Kurth and et al. Exascale deep learning for climate analytics. *SC18: International Conference for High Performance Computing*, 2018.
- [9] NOAA CPC. Merged ir precipitation dataset. http://www.cpc.ncep.noaa.gov/products/global_precip/html/wpage.merged_IR.html, 2024. Accessed: 2024-03-27.
- [10] JR Eyre, W Bell, J Cotton, SJ English, M Forsythe, SB Healy, and EG Pavelev. Assimilation of satellite data in numerical weather prediction. part ii: Recent years. *Quarterly Journal of the Royal Meteorological Society*, 148(743):521–556, 2022.
- [11] Xia Liu and et al. A deep learning framework for atmospheric river detection. *Nature Communications*, 2023.
- [12] George J Huffman, David T Bolvin, Robert Joyce, Owen A Kelley, Eric J Nelkin, Andrea Portier, Erich F Stocker, Jackson Tan, Daniel C Watters, and B Jason West. Imerg v07 release notes. *Goddard Space Flight Center: Greenbelt, MD, USA*, 2023.
- [13] Mary Forsythe. Atmospheric motion vectors: past, present and future. In *ECMWF annual seminar*, pages 1–79, 2007.
- [14] Adriana Romero and et al. Unsupervised deep feature extraction for remote sensing image classification. In *IGARSS*, 2016.
- [15] Kumar Ayush and et al. Generative adversarial networks for surface reflectance generation using multispectral sentinel-2 imagery. *Remote Sensing*, 2020.
- [16] Kaiming He, Xinlei Chen, Saining Xie, Yanghao Li, Piotr Dollár, and Ross Girshick. Masked autoencoders are scalable vision learners. In *Proceedings of the IEEE/CVF conference on computer vision and pattern recognition*, pages 16000–16009, 2022.
- [17] Mathilde Caron, Hugo Touvron, Ishan Misra, Hervé Jégou, Julien Mairal, Piotr Bojanowski, and Armand Joulin. Emerging properties in self-supervised vision transformers. In *Proceedings of the IEEE/CVF international conference on computer vision*, pages 9650–9660, 2021.
- [18] Alexey Dosovitskiy, Lucas Beyer, Alexander Kolesnikov, Dirk Weissenborn, Xiaohua Zhai, Thomas Unterthiner, Mostafa Dehghani, Matthias Minderer, Georg Heigold, Sylvain Gelly, et al. An image is worth 16x16 words: Transformers for image recognition at scale. *arXiv preprint arXiv:2010.11929*, 2020.
- [19] Pascal Vincent, Hugo Larochelle, Isabelle Lajoie, Yoshua Bengio, and Pierre-Antoine Manzagol. Stacked denoising autoencoders: Learning useful representations in a deep network with a local denoising criterion. *Journal of machine learning research*, 11(12), 2010.
- [20] Hugo Touvron, Matthieu Cord, Ishan Misra, and Hervé Jégou. Siamese masked autoencoders. *Advances in Neural Information Processing Systems*, 36, 2023.
- [21] Eric Chen, Diane M Korngiebel, Oluwafemi Olatunji, Neil Thakur, Sean D Mooney, Milena Gianfrancesco, Shawneequa Callier, and Danton Char. Foundation models for generalist medical artificial intelligence. *Nature*, 616(7957):259–265, 2023.
- [22] Zhenda Xie, Zheng Zhang, Yue Cao, Yutong Lin, Jianmin Bao, Zhuliang Yao, Qi Dai, and Han Hu. Simmim: A simple framework for masked image modeling. *International Conference on Computer Vision and Pattern Recognition*, pages 9653–9663, 2022.
- [23] Junnan Li, Pan Zhou, Yongkang Wu, Xiaohan Liu, Hong Liu, and Jiande Gao. Advancing self-supervised learning with efficient transformers. *IEEE Transactions on Pattern Analysis and Machine Intelligence*, 45(5):5843–5857, 2022.
- [24] Qiangqiang Yuan, Huanfeng Shen, Tongwen Li, Zhiwu Li, Shuwen Li, Yumin Jiang, Han Xu, Wancun Tan, Qianqian Yang, Jiwen Wang, et al. Vision transformers for earth observation: A review. *International Journal of Applied Earth Observation and Geoinformation*, 117:103202, 2023.
- [25] Qiangqiang Yuan, Qiang Zhang, Jie Li, Huanfeng Shen, and Liangpei Zhang. Missing data reconstruction in remote sensing image with a unified spatial-temporal-spectral deep convolutional neural network. *IEEE Transactions on Geoscience and Remote Sensing*, 58(8):5362–5374, 2020.

- [26] Qiang Zhang, Qiangqiang Yuan, Jie Li, Zhen Yang, and Xiangli Ma. Missing data reconstruction in remote sensing image with a unified spatial-temporal-spectral deep convolutional neural network. *IEEE Transactions on Geoscience and Remote Sensing*, 56(8):4274–4288, 2018.
- [27] Yanqiu Xing, Mei Wang, Shuyuan Yang, and Licheng Jiao. Missing data reconstruction in remote sensing images with deep convolutional neural networks. *IEEE Transactions on Geoscience and Remote Sensing*, 59(7):5772–5782, 2021.
- [28] Jianwen Wang, Xiangming Xiao, Yuanwei Qin, Jinwei Dong, Geli Zhang, Wei Kou, Cui Jin, Yuting Zhou, and Yao Zhang. Gap-filling of missing data in time series of ndvi images using deep learning. *Remote Sensing*, 12(10):1612, 2020.
- [29] Rui Zhang, Yang Liu, and Hao Sun. Physics-guided convolutional neural network (phycnn) for data-driven seismic response modeling. *Engineering Structures*, 215:110704, 2020.
- [30] Yang Hong, Kuo-lin Hsu, Soroosh Sorooshian, and Xiaogang Gao. Precipitation estimation from remotely sensed imagery using an artificial neural network cloud classification system. *Journal of Applied Meteorology*, 43(12):1834–1853, 2004.
- [31] Robert J Joyce, John E Janowiak, Phillip A Arkin, and Pingping Xie. Cmorph: A method that produces global precipitation estimates from passive microwave and infrared data at high spatial and temporal resolution. *Journal of hydrometeorology*, 5(3):487–503, 2004.
- [32] Phu Nguyen, Mohammed Ombadi, Vesta Afzali Gorooh, Eric J Shearer, Mojtaba Sadeghi, Soroosh Sorooshian, Kuolin Hsu, David Bolvin, and Martin F Ralph. Persiann dynamic infrared–rain rate (pdir-now): A near-real-time, quasi-global satellite precipitation dataset. *Journal of hydrometeorology*, 21(12):2893–2906, 2020.
- [33] Hamed Ashouri, Kuo-Lin Hsu, Soroosh Sorooshian, Dan K Braithwaite, Kenneth R Knapp, L Dewayne Cecil, Brian R Nelson, and Olivier P Prat. Persiann-cdr: Daily precipitation climate data record from multisatellite observations for hydrological and climate studies. *Bulletin of the American Meteorological Society*, 96(1):69–83, 2015.
- [34] Mojtaba Sadeghi, Ata Akbari Asanjan, Vesta Afzali Gorooh, Phu Nguyen, Kuolin Hsu, Soroosh Sorooshian, and Dan Braithwaite. Deep learning methods for satellite-based precipitation estimation: A comprehensive review. *Reviews of Geophysics*, 61(1):e2022RG000815, 2023.
- [35] Hylke E Beck, Ming Pan, Tirthankar Roy, Graham P Weedon, Florian Pappenberger, Albert IJM Van Dijk, George J Huffman, Robert F Adler, and Eric F Wood. Evaluation of 26 precipitation datasets using gauge observations and hydrological modeling. *Hydrology and Earth System Sciences*, 27(9):1865–1881, 2023.
- [36] Neal Jean and et al. Tile2vec: Unsupervised representation learning for spatially distributed data. *ICLR*, 2019.
- [37] Kumar Ayush and et al. Geography-aware self-supervised learning. *CVPR*, 2021.